Journal of Cleaner Production 379 (2022) 134533

Contents lists available at ScienceDirect

Journal of Cleaner Production

journal homepage: www.elsevier.com/locate/jclepro

Full-scale dynamometer tests of composite railway brake shoes including latxa sheep wool fibers

Pablo Monreal-Perez [a,b], Daniel Elduque [a], David López [b], Iranzu Sola [b], Javier Yaben [b], Isabel Clavería [a,*]

[a] Department of Mechanical Engineering, University of Zaragoza, 50018, Zaragoza, Spain
[b] R&D Department, ICER Rail Knorr-Bremse, 31013, Pamplona, Spain

ARTICLE INFO

Keywords:
Sheep wool
Organic fibers
Railway brake blocks
Full-scale dynamometer
Metal pick-up
Life cycle assessment

ABSTRACT

The main target of the present work is to characterize the effect of the inclusion of natural sheep wool (SW) into a railway brake block composition and then to compare it to that of a set of three organic fibers commonly used in the friction material industry: aramid fiber (AF), cellulose fiber (CF) and polyacrylonitrile fiber (PAN). In order to achieve this, 4 versions of the same friction material with a fixed amount of each organic fiber were produced and one more sample was manufactured including no organic fibers. The characterization work consisted of friction tests on a full-scale railway test rig. Then, the samples were SEM analyzed in order to characterize the tested surface microstructure. It was found that all organic fibers helped achieve a more stable bedding, and showed lower friction in wet conditions. They also affected the recovery %. Pictures of the blocks were taken after certain phases of the test and, although the failure sequence remained the same for all samples, the organic fibers very much influenced the magnitude of the wear rates. Sheep wool led to better results than cellulose. No final conclusions could be drawn with respect to metal pick-up. SEM analysis evidenced primary and secondary plateaus, but no significant differences were observed depending on the fiber nature. Finally, a Life Cycle Assessment with a "from cradle to gate" perspective was carried out. Ecoinvent v3.5 database and CML and ReCiPe Endpoint methodologies were used to evaluate the environmental impact create by the five brake block materials. Overall, cellulose, PAN and sheep wool brake blocks show slightly lower environmental impacts that the base material or than aramid fibers. Therefore, Latxa sheep wool offers a good balance between low cost, adequate wear rates and environmental impact, making it a compelling substitute for cellulose fibers.

1. Introduction

The number of environmentally friendly initiatives undertaken has lately been growing larger throughout the different fields comprising both the academia and the industrial sector (Orecchini et al., 2012). One of the reasons for this phenomenon is the genuine concern for the environment sustainability, although it has also been observed that companies can often reach potential benefits by going green. For instance, a green brand image can be linked to brand loyalty (Lin et al., 2017) and it has been found that a percentage of consumers will find appealing an environmentally friendly product that presents an ecolabel or ecological certification, being even willing to pay up to a 20% more for this kind of products (Krause, 2015).

This sort of tendency toward green policies is not new in the friction material manufacture sector. Often triggered by the need for saving costs, there have been many examples of recycled raw materials utilized for a long time now in the friction material field. A clear example are tire peels, that have been often used as an organic filler in friction materials (Singh et al., 2019). Brass chips, which are expected to confer enhanced thermal properties to the friction composite (Bowden, 1951; Kumar and Bijwe, 2010), have also represented a recycled raw material. In early woven materials, brass wire was initially used, but when these materials were reclaimed, the brass wire would become brass chips (Prasenjit et al., 2021). As a handicap, brass chips usually contain traces of lead. Another more recent example of reclaimed raw material is aramid fiber. Often recycled from fire blankets (Manoharan et al., 2019) or bullet-proof vests, the main reason for recycling this component is usually reducing costs. However, there are also examples of raw materials whose use was reduced and which were eventually replaced by others because of the environmental and/or health concerns their use

* Corresponding author.
E-mail address: iclaver@unizar.es (I. Clavería).

https://doi.org/10.1016/j.jclepro.2022.134533
Received 29 July 2022; Accepted 2 October 2022
Available online 6 October 2022

entailed. The main example is the replacement of asbestos for other types of fibers when it was proven to cause health issues and respiratory conditions (Uibu et al., 2004; Ospina et al., 2019). Also, solvents, which constituted an important process aid by making raw materials available for reaction during the friction material manufacture, found their use advised against in some cases because of their environmental impact (Cox, 2012a). As for lead, it has been used in sintered metals and semi metallic friction formulations (Batchelor and Carey, 1954) and has been found to be a friction stabilizer (Wild, 1931) and a solid lubricant (Shimer, 1883), but its use is now not allowed due to this metal's toxicity (Prasenjit et al., 2021). Other components are also being substituted, like copper, tin, antimony trisulfide or whisker materials (Bijwe, 2016).

But leaving aside the active work oriented to removing hazardous raw materials from the brake composition, there are other areas of relevance within the field of environmentally friendly friction materials. Examples to this regard are the brake emissions, which are to be minimized (Kunz et al., 2019), or the use of raw materials to reduce waste disposal. For instance, the use of recycled nitrile butadiene rubber (NBR) has prevented it from ending in landfills (Spokes, 1947). This last option is closer to one of the new approaches being tackled and that entails the use of agro-waste as raw materials, such as the palm kernel shell (Talib et al., 2017) or the areca sheath (Sai et al., 2019). These sustainability claims should be properly analyzed, performing a Life Cycle Assessment (LCA), in order to quantify the environmental impact. LCA is based on ISO 14040 (ISO, 2006a) and 14044 (ISO, 2006b), and provides a scientific, systematic and objective methodology to calculate the environmental impact of product, processes or services. Although LCA is widely used methodology, and has been applied to a wide range of products such as electric vehicles (Murat et al., 2022), metro trains (Del Pero et al., 2015) or railway infrastructure (Batista et al., 2022), there are not many example of LCA of train brake components. Gradin and Åström performed a comparative LCA of car disc brake systems, finding that material mix in the friction pads were relevant in the overall impact (Gradin and Åström, 2020). Madeswaran et al. assess "Eco-Friendly" automotive brake pads but without performing a proper LCA. In that paper, the "Eco-Friendly" claims were only based on the fact that the pads were asbestos-free and used kenaf fibers (Madeswaran et al., 2016).

The present piece of research explores this way of using raw materials without other possible use by including sheep wool in the formulation of railway brake blocks in exchange for other organic fibers. Thus, latxa sheep wool has been used to study to what extent this material can successfully develop the role of organic fibers within a brake shoe. The latxa sheep (ovis aries) is a sheep breed autochthone to the Spanish regions of Navarre and the Basque Country, where it is grown primarily for meat and dairy products. However, its wool is currently not demanded for textile production due to its high resistance and toughness. This leads farms to turn to specialized companies for the calcination treatment of these residues. The use of this material in the friction sector would mean a reduction of these calcination processes, as this waste will be used as a raw material, while also contributing to the growth of a local circular economy. In addition, it would also bring economic benefits to the farms, as they would find savings in treating lower amounts of waste. In fact, this constitutes a current affair and there exists a number of proposals being developed in this direction by different entities (Jordan, 2020; Tejada, 2020). Companies could be interested in collecting wool at zero cost as the brake manufacturer would also encounter profits in doing so. Beyond selecting the best wool portion and cutting it to a suitable fiber size, this raw material does not require any further treatment, which would mean savings while not having to invest in the purchase of the common organic fibers such as cellulose. In addition, considering that just Navarre has more than 63,000 heads of sheep for dairy product production alone, and that each sheep can produce more than 3 kg of wool per year, only this region would easily represent a potential supply of about 189,000 kg of wool per year.

Specifically, and from the technical perspective, a complete characterization is carried out on the effect of natural sheep wool fibers on the wear and friction performance of railway brake shoes in a full-scale railway inertia dynamometer. The characterization is also run on brake blocks using typical organic fibers such as aramid, cellulose and polyacrylonitrile (Cos, 2012). Fibers such as aramid and polyacrylonitrile have relatively high cost, therefore natural fibers are attracting much interest as potential alternative to these synthetic fibers (Arman et al., 2007; Huang, 2009; Shalwan and Yousif, 2013; Aranganathan et al., 2016).

For five brake blocks, the full-scale dynamometer tests included a wide range of speeds, braking forces and tonnages in dry/wet conditions. Then, a Life Cycle Assessment has been carried out. All these results are then compared in order to prove the suitability of this natural raw material, new in the friction field.

2. Material and methods

2.1. Preparation of samples

The three commercially available organic fibers employed were purchased from two suppliers. The sheep wool was collected at a local farm and was not treated beyond the manual cut required for the fiber length to be acceptable, comparable to that of other fibers and processable. Values of fiber length were available on the technical data sheets by the suppliers for the aramid, cellulose and PAN fibers. In the case of the sheep wool, this parameter was measured with a Nikon SMZ800 optical microscope, along with a HY-1448 microscope led light and a Zuzi UCMOS microscope camera. The density values were determined by weighing fixed amounts of each fiber sample and then measuring their volumes with a test tube according to an internal test method at Knorr-Bremse. This data is shown in Table 1.

Fibers typically presented similar values of density. Sheep wool seemed to present a slightly lower value, although not significantly. This is probably due to the fact that it was the only fiber that was not compressed in its package for delivery. In terms of fiber length, PAN and sheep wool presented the largest values.

Within this research work, five different variations of a base friction material were prepared. First, a pre-mix was produced by mixing typical raw materials to be found in brake compositions. These raw materials included nitrile butadiene rubber (NBR, that can improve the mechanical properties of composite friction materials, as well as wear resistance, friction coefficient and damping braking noise (Fei et al., 2015; Surojo et al., 2019), steel fiber (the most widely used metallic fibers in friction materials, Kalel et al., 2021, can have effect in both the friction performance and wear of the friction material in which it is used, Matějka et al., 2009), barites (a very common filler, Kumar and Kumar, 2020, that is important in the formation of a stable transition layer, Menapace et al., 2018, and substantially influences the friction coefficient and specific wear ratio, Sugözü and Dağhan, 2016), magnesium oxide (a soft abrasive which can serve as a wear reducing filler when in presence of more aggressive abrasives and can act as an accelerator, speeding up the rubber vulcanization, Singh et al., 2020) or zircon (an abrasive that can lead to heat resistance at elevated temperatures, Park et al., 2021), affect the friction stability depending on its particle size and modify the friction material wear rate, Shin et al.), among others (Monreal et al., 2021a). These constituents were mixed for 2 min in a laboratory-scale powder disperser, which comprised of a cylindrical steel container with four spinning blades at its bottom. Given the nature of the mixer at hand, the NBR rubber component was selected in a powder form. Each

Table 1
Density and fiber length for the 4 organic fibers tested.

Fiber	Aramid	Cellulose	PAN	Sheep wool
Density (g/cm3)	0.14	0.14	0.11	0.10
Fiber length (mm)	1.5	0.9	3	1–7

one of the samples was prepared following the compositions collected in Table 2. The selected organic fibers were added in constant volumes of 15% and then further mixed along the pre-mix for 2 more minutes in the previously mentioned mixer.

Finally, the mixes were molded into railway brake shoes of 320 mm × 80 mm x 60 mm at room temperature. The pressing cycle lasted 3 min and entailed a force of 800kg/cm2. Then, the green blocks were cured in a laboratory scale batch oven for 24 h at 140 °C.

2.2. Characterization of friction materials and friction tests

Samples were taken from the different friction materials produced and then tested both physically and mechanically. As for the friction tests, the five different materials were characterized in one of the full-scale railway brake dynamometers at Knorr-Bremse, shown in Fig. 1. All tests followed procedures previously reported (Satapathy and Bijwe, 2004).

A single brake block was tested, that is, in 1xBg configuration. In the picture, (a) a railway wheel is observed. The brake block is inserted in the brake block holder which is attached to the tread brake unit (b). The torque generated by applying the brake is measured with a load cell column (c) attached to the dynamometer frame (d). Thermocouples were also placed in contact with the wheel tread so the evolution of the temperature could be recorded and, finally, assessed. The testing program comprised of a more complete set of braking stops, as shown in Table 3.

Also related to the friction results, fade and recovery were evaluated. Fade is the loss of braking effectiveness at certain conditions such as high temperatures, and recovery represents the ability of the break to present a normal friction when conditions have returned to the originals (Saffar and Shojaei, 2012). Recovery percentages were calculated as shown in equations (1) and (2), and fade was obtained as in expressions 3 and 4 (Kim et al., 2001):

$$\text{Drag brake recovery } (\%) = \frac{\mu_E}{\mu_C} \cdot 100 \quad (1)$$

$$\text{Thermal phase recovery } (\%) = \frac{\mu_G}{\mu_E} \cdot 100 \quad (2)$$

$$\text{Drag brake fade } (\%) = \frac{\Delta\mu_D}{\overline{\mu_D}} \cdot 100 \quad (3)$$

$$\text{Thermal phase fade } (\%) = \frac{\Delta\mu_F}{\overline{\mu_F}} \cdot 100 \quad (4)$$

Where μ_C is the average friction for each material at high speeds and high braking forces during phase C, μ_E during phase E, and μ_G during phase G. This way, for each the drag brake and the thermal phase both the previous and the next phases are considered in the calculation of recovery. $\Delta\mu_D$ and $\Delta\mu_F$ are the difference between the maximum and the minimum friction coefficient per brake stop during phases D and F respectively. Finally, $\overline{\mu_D}$ and $\overline{\mu_F}$ are the average friction coefficient during phases D and F respectively.

Table 2
Compositions of the 5 friction materials in volume percentage (volume %).

Component	Friction material 0 (%)	Friction material AF (%)	Friction material CF (%)	Friction material PAN (%)	Friction material SW (%)
Friction material pre-mix	100	85	85	85	85
Aramid fiber	–	15	–	–	–
Cellulose fiber	–	–	15	–	–
PAN fiber	–	–	–	15	–
Sheep wool	–	–	–	–	15

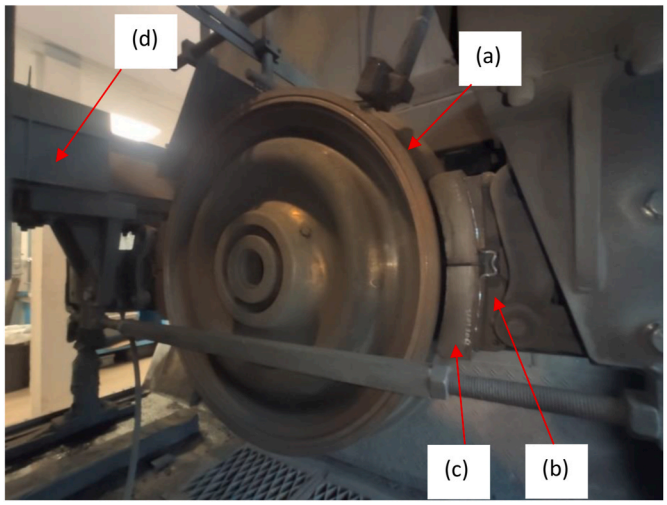

Fig. 1. Full-scale railway dynamometer.

Table 3
Briefing of the test conditions used in the friction test procedure.

Test phase	Description
Bedding	Bedding + dry braking + conditioning stops
A	Dry, empty load, various braking forces and speeds
B	Wet, various loads braking forces and speeds
C	Dry, full load, various braking forces and speeds
D	Drag brake
E	Friction coefficient check: Dry, full load, various braking forces and speeds
F	Thermal phase: Dry, full load, initial temperatures at 150°, 200° and 250 °C
G	Friction coefficient check: Dry, full load, various braking forces and speeds

A bedding was kept as the initial phase at constant conditions that could grant a contact surface between the brake blocks and the wheel over the 90% of the block's area. Braking stops were carried out at different conditions of initial speed (from 30 to 120 km/h), braking force (from 5 to 38 kN), load (empty: 2,5 tons/loaded: 11 tons) and environment (dry/wet).

The SEM analysis on the tested brake blocks was carried out on a HITACHI S4800 scanning electron microscope with an Oxford EDX detector.

2.3. LCA methodology

The aim of this Life Cycle Assessment is to analyze the environmental impact of a brake block that can be manufactured out of the five previously mentioned friction materials. To analyze the influence of the material composition, a functional unit of one unit of brake block, considering a "from cradle to gate" approach has been proposed. This cradle to gate approach includes raw material acquisition, transportations to the factory, and the production processes needed to manufacture the brake blocks. Each brake block final weight is shown in

Table 4
Brake block weights.

	Friction material 0	Friction material AF	Friction material CF	Friction material PAN	Friction material SW
Weight per unit (Kg)	3.47	3.23	3.27	3.24	3.30

Table 4, as they differ slightly depending on the composition.

The LCA is performed, following ISO standards 14040 and 14044 (ISO, 2006a, 2006b)], and using two environmental calculation methodologies: CML-IA baseline v3.05 and ReCiPe 2016 Endpoint (H/A) World (2010) v1.03 (Huijbregts et al., 2016; Pre Consultants, 2020) CML provides a Midpoint Analysis, which is useful to analyze a wide range of environmental categories, whereas ReCiPe Endpoint also consider a wide range of categories, but normalizes and performs a weighting step to add up all the results into a single score, which allows for easier interpretation (Dong and Thomas, 2014). The (H/A) World (2010) ReCiPe version is the default method, that uses the "Hierarchist" perspective, Average weighting sets and global normalization factors for the year 2010. The software used to perform the calculations is SimaPro v.9.0.0.49 (Pre Consultants, 2020).

In order to carry out an LCA, first a Life Cycle Inventory has to be performed for the five friction materials. The LCI is based on primary data, and EcoInvent v3.5 has been selected as the reference database. EcoInvent is one of the most used LCI databases, and is developed by the Swiss Centre for Life Cycle Inventories (Wernet et al., 2016).

The manufacturer has provided primary LCI data of the material composition, the transportations to the factory, and the production processes. However, they cannot be provided in full detail due to confidentiality reasons. A summary of the main materials used for the 5 different brake block compositions was provided in Table 2. Although the exact percentages cannot be provided, the main materials used, and the used Ecoinvent datasets are provided in Table 5. Assignment between the life cycle inventory data, and the EcoInvent datasets was performed following Ecoinvent Guidelines (Wernet et al., 2016). Regarding the manufacturing process, information is given in section 2.1 Preparation of samples. .

Latxa Sheep Wool is currently a waste stream in the agricultural sector. Instead of being calcined, as it is common practice, the manufacturer is now using it as a raw material for the brake block manufacturing. In order to evaluate the environmental impact of the wool, a conservative approach has been considered: the avoided waste incineration treatment has not been considered as "credit" for the LCA, and the environmental impact of the wool has been calculated as the impact of the transportation from the farm to the factory. The average distance from the farms is 20 Km, and the transportation is carried out by a small size truck. "Transport, freight, lorry 3.5–7.5 metric ton, euro5 {RER}" has been selected to this transportation.

For all the rest of materials, the transportation from the suppliers to the factory (Navarre, Spain) have been considered, as shown in Table 6. Exact distances are not provided due to confidentiality reasons. The Ecoinvent dataset "Transport, freight, lorry >32 metric ton, euro5 {RER}" has been used for truck transportation, where as "Transport, freight, sea, transoceanic ship {GLO}" has been selected for freight ship transportation.

Table 5
Main materials and Ecoinvent datasets for the brake blocks.

Material	EcoInvent dataset
Zircon	Zircon, 50% zirconium {RoW}| heavy mineral sand quarry operation
Magnesium oxide	Magnesium oxide {RER}| production
Barite	Barite {RER}| production
Coke	Coke {GLO}| market for
Glass fibre	Glass fibre {RoW}| production
Steel fibre	Steel, unalloyed {GLO}| market for
Sulphur	Sulphur {GLO}| market for
NBR	Acrylonitrile-butadiene-styrene copolymer {RER}| production
Phenolic resin	Phenolic resin {RER}| production

Table 6
Main materials and transportation distances.

Material	Main means of transportation
Zircon	Freight Ship
Magnesium oxide	Truck
Barite	Truck
Coke	Truck
Glass fibre	Freight Ship
Steel fibre	Truck
Sulphur	Truck
NBR	Truck
Phenolic resin	Truck
Latxa Sheep Wool	Small size truck

3. Results and discussion

3.1. Physical, chemical properties of friction materials

After the curing cycle, all friction materials were characterized. The results obtained are presented in Table 7. No significant differences were found in terms of shear force (the effort necessary to detach the friction material from the backing plate) or hardness. As it was expected, the addition of any kind of fiber brought a decrease in the density, being material 0 the denser material. All materials containing organic fibers showed similar density values as they were added in the same volume percentage. The acetone extractable did not significantly change coinciding with previous works (Satapathy and Bijwe, 2004). The compression test gave results for the maximum load until failure and the young modulus. The maximum load for the friction material containing aramid fiber was the highest, which is in concordance with previously reported results on aramid fiber enhancing the friction material mechanical properties and resistance to crack appearance and propagation (Kim et al., 2001), although the difference was not significant. Also, for all friction materials with fibers in their composition, the young modulus dropped when compared to that of the control friction material as it did in previous works with these materials (Monreal et al., 2021b).

3.2. Friction characterization

The friction characterization started test phase "bedding" in which significant differences were observed for the friction material 0 (using no organic fibers) when compared to the other 4 friction materials, as shown in Fig. 2. The brake blocks had not their radii mechanized to fit the wheel, so the friction surface varied over the bedding phase up to a minimum of 90% of the blocks' area.

Material 0 commenced the test at the same friction level that the other samples. Then, its friction dropped only to grow higher and take values as high as 0.4 at the end of the 50 stops comprising the first stage of the bedding. The level of friction kept high for the following 6 stops at high speed and high braking force. The dispersion with changing speeds was also higher for material 0. After that, the friction coefficient decreased, slowly approaching the friction level of the other samples during the conditioning stops at the end of the first stage of the test. All samples with organic fibers showed a constant, stable friction level that can be classified as that of a K block. No significant differences were observed between any of them which seems to point to the presence of this type of raw material as an advantage while looking for a more stable friction (Cox, 2012b). The organic fibers might have been helping achieve a steadier wear, as it has previously been reported that the friction performance can evolve specifically over the bedding phase depending, for instance, on the sustainability of the transfer layer (Wu et al., 2011).

In terms of the dependence of the friction performance on different testing conditions, several cases are shown in Fig. 3. This data was collected during test phases A, B and C. In terms of load, both cases (empty and full load) are considered on the graphics. When the friction coefficient was studied depending on both the brake application force

Table 7
Physical and mechanical properties of the friction materials after curing.

Friction material	Shear force (kg/cm^2)	Shore hardness (−)	Density (g/cm^3)	Acetone extractable (%)	Maximum load (MPa)	Young modulus (MPa)
Material 0	34	69	2.22	1.57	27.9	415
Material AF	34	67	2.08	1.78	32.5	310
Material CF	34	67	2.09	1.58	25.9	280
Material PAN	33	59	2.05	1.69	31.9	170
Material SW	33	64	2.08	1.62	27.5	175

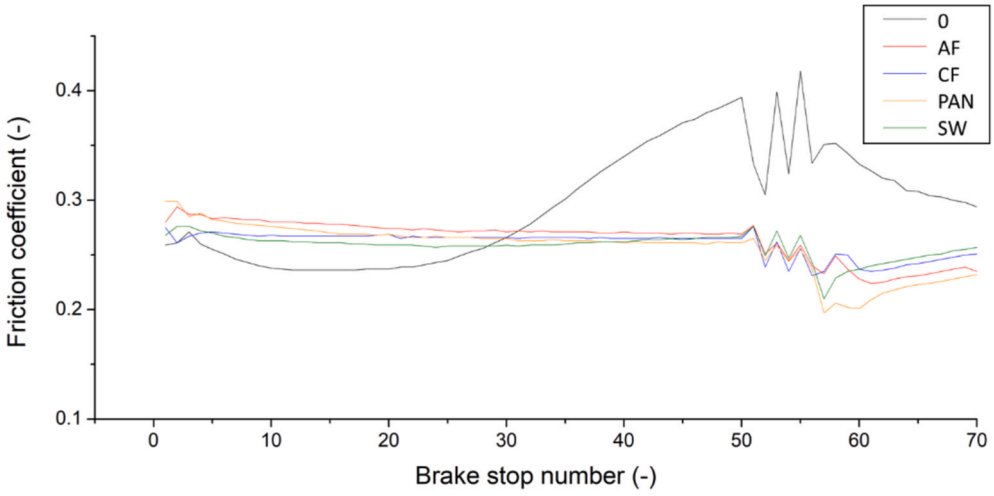

Fig. 2. Average friction coefficient per brake stop in chronological order over the initial phase (bedding).

and the initial speed, generally all friction materials showed a lower friction in wet conditions. This behavior of friction materials in presence of water can be easily found in literature (El-Tayeb and Liew, 2009), and can often result in lower wear (Gibson and Taccini, 1989) and changes on the friction range due to the different wear mechanisms that this particular environment brings with it. Among other aspects, water has been reported to prevent to a certain degree the formation of transference layers, char and oxides in the interface, as well as to accelerate the plateau structure disintegration ((El-Tayeb and Liew, 2008). But this is not exclusive of friction materials, and it motivates studies in areas within the railway braking field not directly including the friction elements, such as those concerning the rail-wheel adhesion (Chen et al., 2011). Also, a fairly wide dispersion can be found in results obtained in wet conditions. This happens both for the friction results of a given sample and the friction data of the different materials when compared with each other. An example to this regard can be found in Fig. 3(d), where the friction materials tested gave different friction coefficients within a very narrow range of brake application forces. This can be related to the friction coefficient variation mechanism in wet conditions. Hypothesis have been tested with regards to his matter suggesting the possibility of debris agglomerates being jammed in the gaps between the friction surfaces (Matsumori et al., 2016).

Aside from that, no vast differences were found between the different samples, but in general terms, friction material 0 presented slightly higher friction than the other samples in all scenarios, but particularly at high speeds in wet conditions as can be observed in Fig. 3(b). None of the friction materials including organic fibers presented significant differences when compared with each other. Variations of friction with both the speed and the brake application force were subtle, but in the two cases AF presented the highest ones in dry conditions: and 15.5% and 10.3% respectively in Fig. 3(a) and (c). The slightly lower friction that AF showed in certain scenarios could be related to its lower wear rate and the reduced amount of work that goes with it (Kato and Magario, 1994). As for material containing sheep wool, its friction coefficient varied in a similar range to those of CF and PAN. Friction material 0 was the most stable with speed changing. In general terms, the friction results obtained in a railway full-scale dynamometer can relate to a level to those from a mid-scale dynamometer (Monreal et al., 2021b). In a previous research work by the authors using this type of smaller dynamometer, much less demanding braking conditions were evaluated, but a very similar friction level was observed for all friction materials including organic fibers with speed changing. The slightly higher result dispersion when assessing the friction coefficient as a function of the braking pressure was also observed.

The maximum temperature was also studied. As it can be seen in Fig. 4(a) and (b), the operating parameters, especially the initial speed, influenced the results in a more marked way than the differences in composition. This sort of effect has previously been reported in some research studies concerning organic fibers (Satapathy and Bijwe, 2006). Nevertheless, it can be seen that the friction material including PAN fiber would typically reach higher temperatures than the rest of samples, while SW material showed to behave oppositely at high braking forces and high initial speeds. The largest difference in temperature between the two materials reached 50 °C (297 *vs* 247 °C at high braking forces). Even though this difference is not this wide in all tested scenarios, and no significant differences were found in friction coefficient as mentioned before, it is known that at 300 °C some binders such as straight phenolic resins reach their thermal decomposition temperature and the wear rates of the friction materials they are part of, start rapidly increasing (Hong et al., 2009). In addition, performing above or below the thermal decomposition of the binder triggers changes in the friction mechanism (Jara and Jang, 2019). These facts should be kept in mind when selecting an organic fiber to be included in a resin-based friction material. As for Fig. 5, it can be observed that regardless of the nature of the organic fiber being used, no special differences were found in terms of friction coefficient variation with the temperature. This could appear to be in contrast with the maximum temperatures commented before, but the friction stability can be explained by the pre-mix composition. This fraction of the brake shoes makes all samples rubber-based friction materials, which have been reported to present less temperature fade

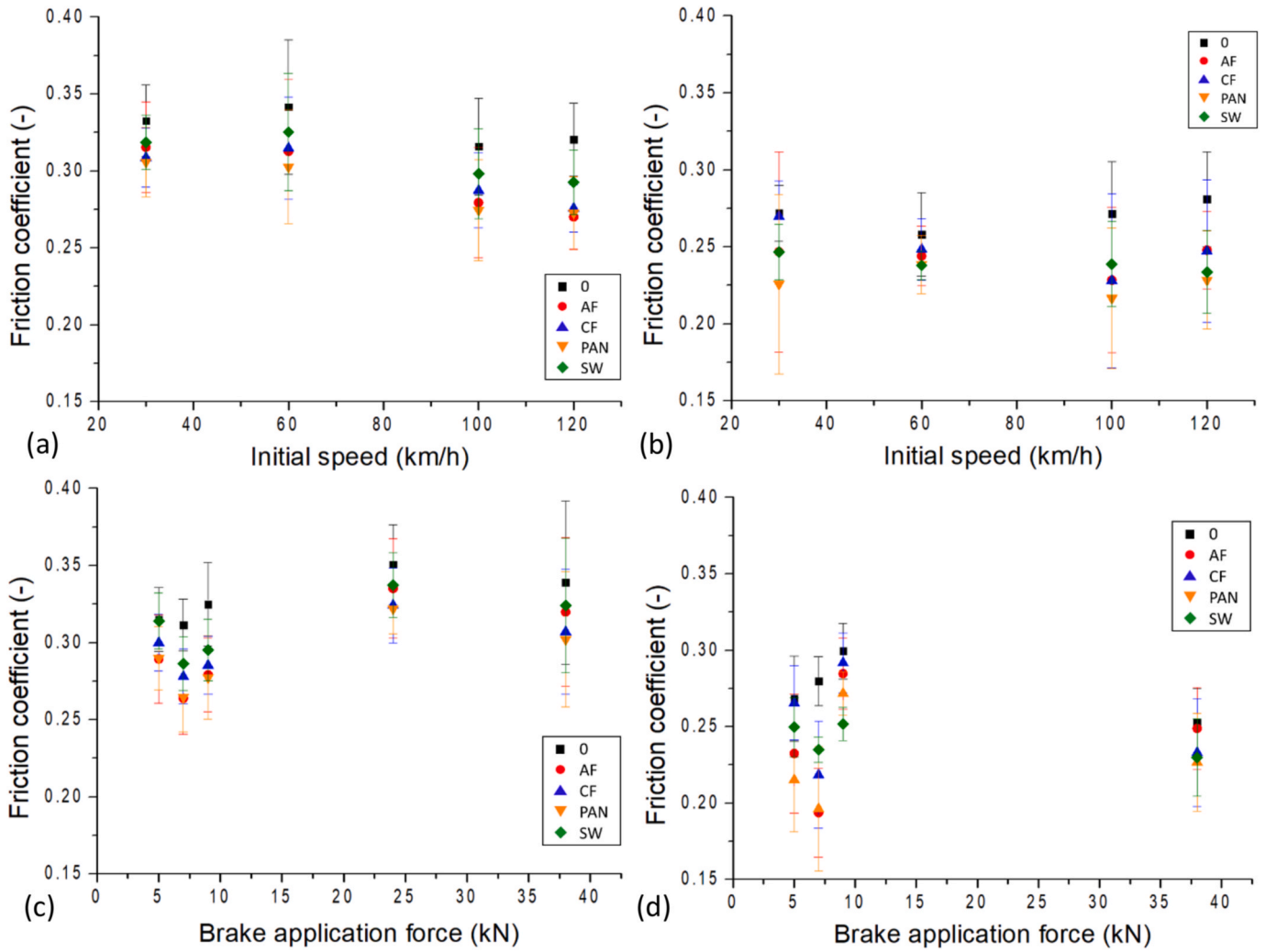

Fig. 3. Variations of the average friction coefficient with (a) initial speed in dry conditions, (b) initial speed in wet conditions, (c) braking force in dry conditions and (d) braking force in wet conditions.

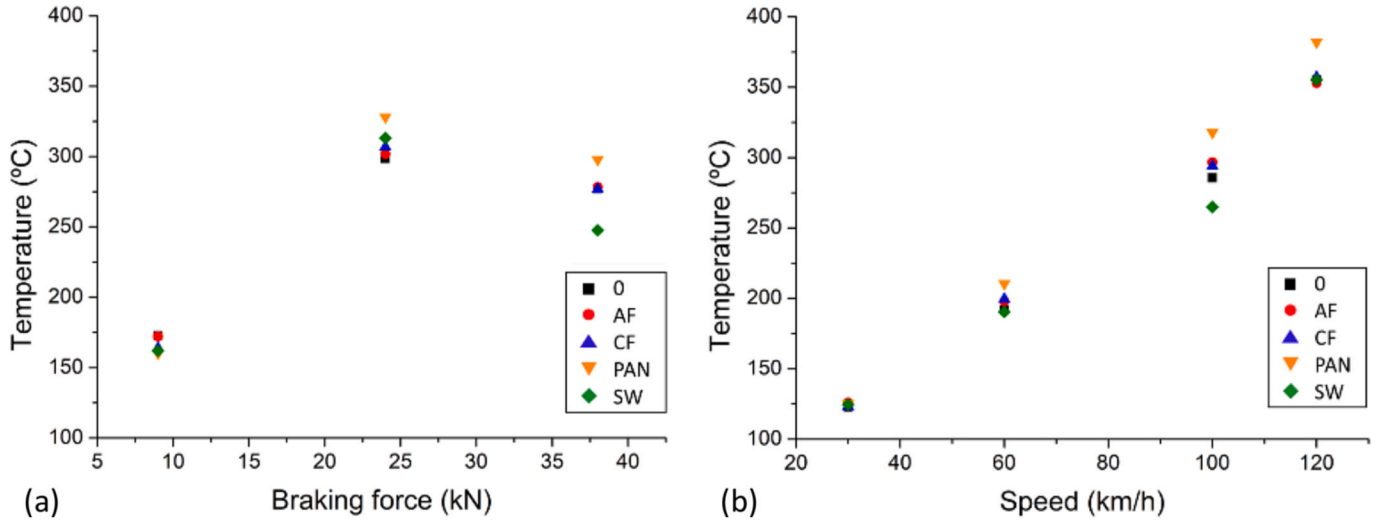

Fig. 4. (a) Maximum temperature vs braking force and (b) maximum temperature vs initial speed.

than those based on resins (Saffar and Shojaei, 2012). It also makes that all samples share the same friction modifiers, which play a more important role in braking and seem to have conferred the shoes a good friction stability.

On the drag brake (test phase D), the brake blocks were applied to the wheel for 2040 s at a constant speed of 70 km/h. The engine prevented

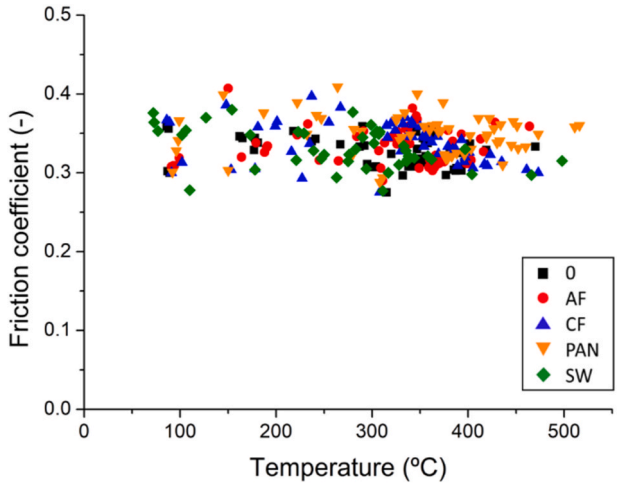

Fig. 5. Average friction coefficient per brake stop vs the maximum temperature reached.

the wheel from stopping and the instantaneous friction coefficient was recorded. Fig. 6 shows the friction coefficient and the average temperature evolution with respect to time. No significant differences were observed in this phase of the experiment in terms of friction performance: first the samples presented a stable coefficient, then a drop in friction after around 150 s, after which it increases in all cases to a coefficient of 0.35. AF and PAN were the only materials showing slight differences in this last rise of friction, while CF and SW were the ones performing the closest to the base material. All friction materials showed virtually the same friction level at the end of the drag brake phase with temperatures between 500 and 550 °C. This makes sense since all organic fibers have decomposed by this point, even the aramid fibers can start decomposing at temperatures over 500 °C (Li et al., 2018).

As for recovery, values close to 100% are preferred for good friction performance, since it means that after given brake stops, the brake will still perform the same. In the present work, percentages differed up to a 20% between materials as can be seen in Fig. 7(a). While the thermal phase (test phase F) did not bring large variations in the recovery % with samples including organic fibers giving values between 105% and 110% (similarly to previous results in smaller scale friction tests, Sarapathy and Bijwie, 2004), the drag brake seemed to affect differently friction material 0 and the one including PAN. They gave the lowest (94.6%) and the highest (117.7%) recovery percentage respectively. SW material, on the other hand, showed the closest recovery to 100%. On fade, the phase affecting the friction materials the most was the drag brake, once again, as it shows in Fig. 7(b). The fade results for this phase were basically determined by their friction coefficient at the beginning of the brake stop, since all of them came to present the same friction in the end. The PAN material showed the highest fade, which might be linked to its recovery being the highest. This material seems to find its composition altered at the demanding conditions of the drag brake so that its friction is increased. On the other hand, the thermal phase affected fade to a lower degree, as it happened for recovery. This phase is more relatable (differences on the absolute values aside) to the thermal phase tested in a mid-scale railway dynamometer. To this regard, AF showed again the highest fade (Monreal et al., 2021b) and the PAN material also showed the closest fade to that of the control material (Sarapathy and Bijwie, 2004).

3.3. Wear and block integrity

The tested brake shoes were checked after phases B, D, F and G. One of the aspects noticed was the presence of metal pick-up on all the tested samples. Along with other defects, brake blocks are known to develop metal pick-up in certain cases. This is an incidence consisting on the presence of iron lumps trapped on the friction surface of the friction material. They tend to show an iron oxide interface and are influenced by temperature (Nukumizu et al., 2008). However, the most influencing factor on the appearance of this transference of material is often a wet environment (SAnitate and Schmitt, 2008). As it can be observed in Fig. 8, these metallic inclusions reached significant sizes of 110 mm long or 40 mm wide in the worst cases after the demanding conditions of phase B. Two types of defects are marked on Fig. 8: metallic inclusions are indicated in blue circles, and pits are pointed using red lines. It is speculated that all samples developed metal pick-up to a similar degree and that the holes marked in red were once filled with metal. The metallic particles could have been let go as seem to show the areas marked with both colors. The metallic inclusion on material 0 was the widest. Also, PAN material barely presented empty pits and showed the longest metallic particles. Unfortunately, it could not be stated whether PAN material was actually showing a higher level of metal pick-up than other samples, or if it would have let the iron lumps go if tested for a longer time.

In terms of wear rates, significant differences were found depending on the organic fiber used in each sample. In Table 8, the average wear

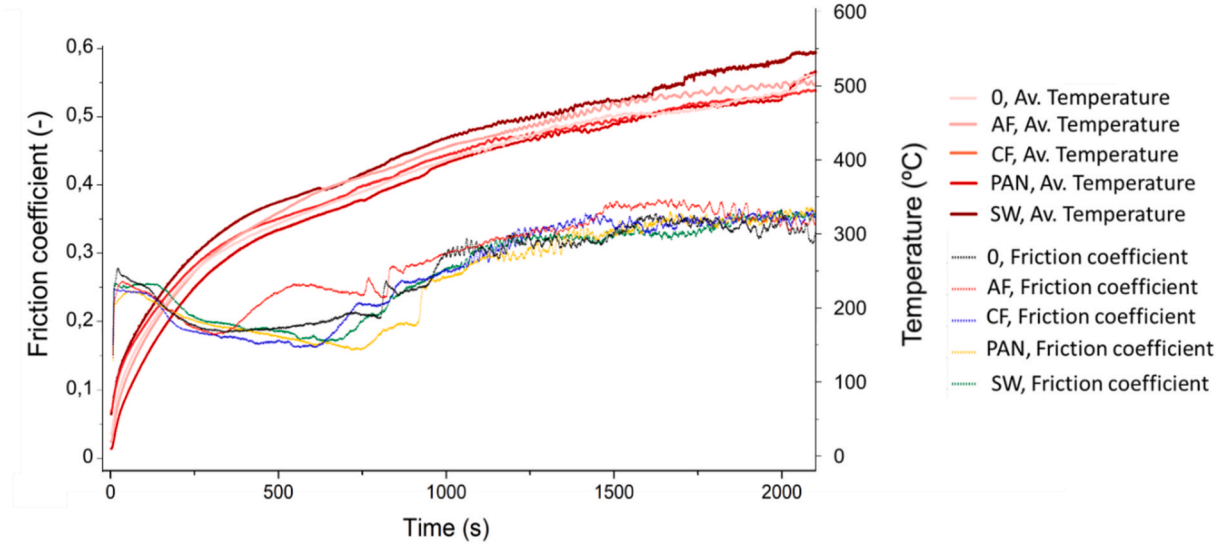

Fig. 6. Instantaneous friction coefficient and temperature evolution over time during the drag brake application (phase D).

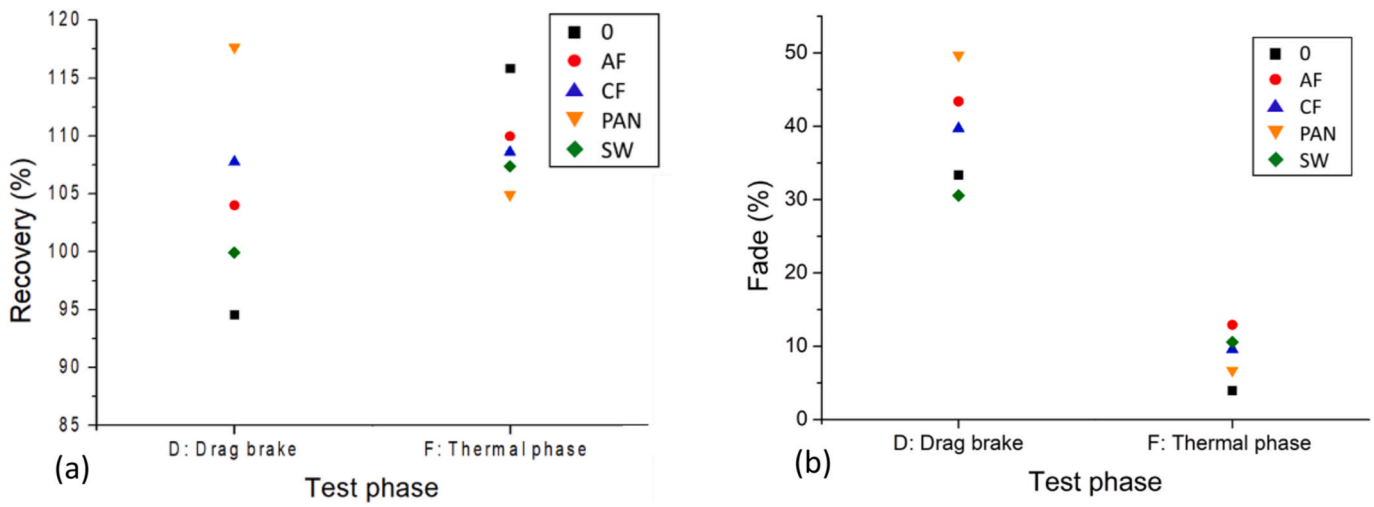

Fig. 7. (a) Recovery and (b) fade percentages of the tested materials for the drag brake (D) and the thermal phase (F).

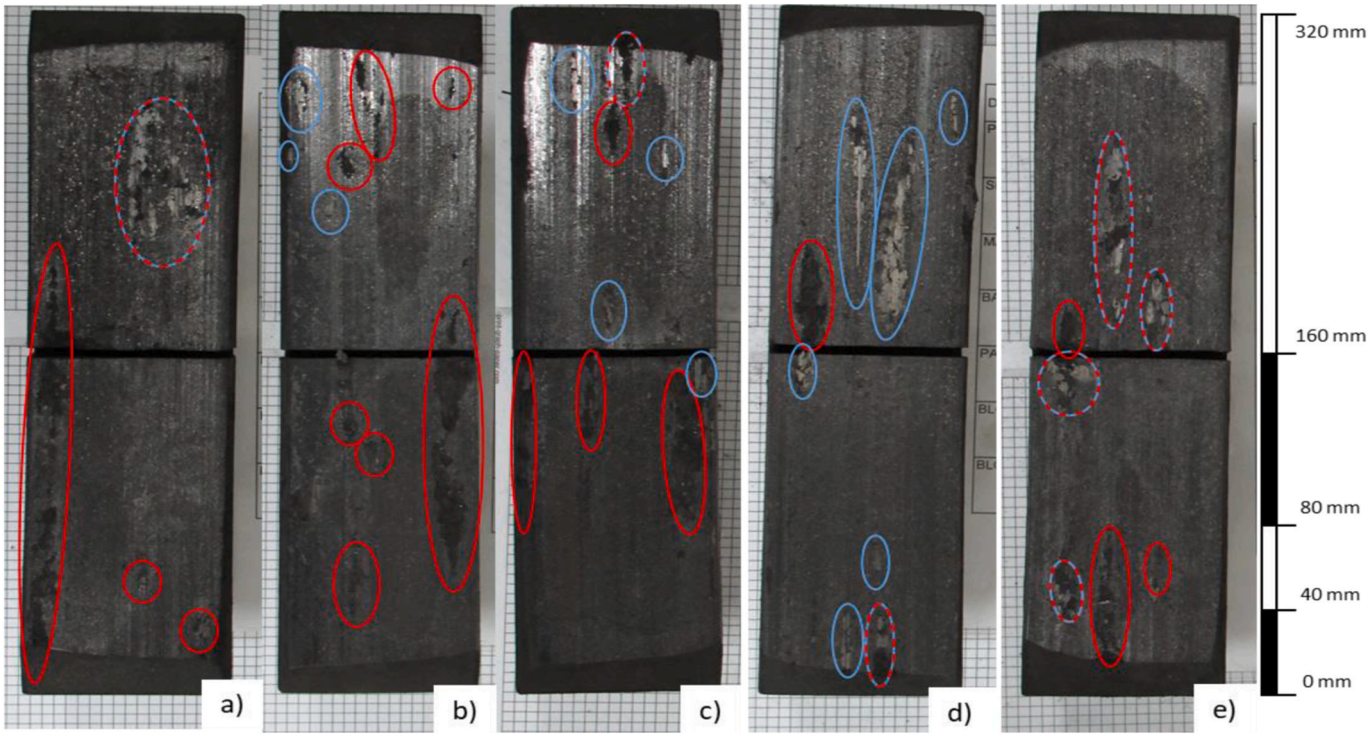

Fig. 8. Pictures after test phase B in wet conditions of (a) material 0, (b) material AF, (c) material CF, (d) material PAN and (e) material SW.

Table 8
Wear rates for the tested brake blocks for different test phases.

Wear rates (cm^3/MJ)	Material 0	Material AF	Material CF	Material PAN	Material SW
Phases C and D (drag brake)	1.15	1.10	1.40	1.10	1.16
Phases E and F (thermal phase)	0.65	0.96	2.81	1.30	1.52
Global (average of all phases)	0.37	0.45	0.88	0.52	0.58

rate for the entire test plus the specific rates for the parts of the program including the most demanding phases (drag and thermal phase) are collected.

In all cases, material CF showed the largest rates, especially during the thermal phase. These results are coherent with the thermal stability shown by the individual fibers in TGA tests (Monreal et al., 2021b), where cellulose fiber was the one showing the weakest stability, followed by the sheep wool, the PAN and the aramid fibers. This order matches the wear rates shown by the friction materials during the thermal phase. Material 0 showed the lowest rate, followed by materials AF and PAN, unlike during the drag brake, where wear rates showed to be relatively similar for materials 0, AF, PAN and SW. It can be found in literature that the addition of 3% of aramid, carbon and PAN fibers can provide a drastic reduction in wear (Satapathy and Bijwe, 2004), but the present research work proves that when using higher percentages of

aramid fiber and friction materials are subjected to demanding conditions, this does not extrapolate. Research works corroborate this higher wear of friction materials including concentrations of this fiber (Cai et al., 2015).

However, the wear mechanism seemed to be very similar as the friction materials presented the same failures after the same phases. Some of the common failure modes in friction materials tested in real conditions were observed in all pieces tested (Laguna-Camacho et al., 2015). These included pits (al seen in Fig. 8), fatigue, thermal cracks and, eventually, a vast case of delamination. Material SW is shown as an example in Fig. 9. After the drag brake, all samples showed a flattened surface. The binder seemed to have melted along with debris and other components of the brake, generating a fairly thick layer that even completely covered the blocks' grooves. Also, when studying the side of the blocks, a long thermal crack showed, especially from the center towards one of the ends of the shoes, as shown on the left side of the red line in Fig. 9(a). At the extreme conditions of the drag brake, all brake blocks tested reached 515-530 °C. This explains all samples presenting the melted-like aspect of picture 9(a). Even the aramid fiber, which is known for its outstanding thermal stability, did not represent an advantage when it comes to the shoe's integrity, as it melts into a viscous, glassy substance at 500 °C (Satapathy and Bijwe, 2004).

After the friction coefficient check (phase E), the shoes underwent the thermal phase of the test, where the temperatures were also high but unlike in the drag brake, the temperature was allowed to decrease to specified values (150 °C, 200 °C and 250 °C) after each brake stop. These cycles seem to have brought a significant amount of stress and fatigue onto the surface of the brake shoes, which eventually broke on the cracked side and pieces of different sizes fell off as shown in Fig. 9(b). This fact may have signified an important contribution to the wear loss over the thermal phase. Although all samples showed this wear sequence, it can be seen that, coinciding with the poorest thermal stability of cellulose (Satapathy and Bijwe, 2004), material CF presented a significantly higher wear rate during the thermal phase, even doubling that of material SW, the second most wearing material.

3.4. Microstructure

After the friction test, samples were taken from the different brake shoes and SEM tested. SEM images can be observed in Fig. 10. The organic fibers were not appreciable on the worn surfaces and EDX did not help, due to their carbon structure or the fibers. Differences on the wear mechanism could not be stated for the diverse samples analyzed. This is in concordance with all the brake shoes presenting the same failure modes and defects during the friction test and seems to point out that the organic fiber does not represent a modification on the wear mechanism. Particularly, this mechanism appears to consist of plateau structures, both primary and secondary. These plateau systems have been documented by Eriksson et al. (Eriksson and Jacobson, 2000; Eriksson et al., 2002) and typically consist of components of the friction materials that are more difficult to remove by the effect of friction (primary) and that make easier for debris and worn off material to form agglomerates (secondary plateaus). The tested samples presented regions showing both only primary plateaus and primary plateaus serving as support to secondary plateaus. Examples of primary plateaus can be observed in Fig. 10(a) and (b). In both pictures steel fibers (marked with the iron symbol, Fe) are seen to have been deformed which is confirmed by their flatter surfaces. The braking direction is indicated in blue arrows. On the other hand, secondary plateaus can be evidenced by primary structures in Fig. 10(c) and (d). In these images, MgO particles are always marked with red circles, and debris accumulations in green ones. It can be observed that even though steel fibers tend to protrude and be more tightly fixed to the friction material surface, abrasives such as zircon or MgO, along with other components as coke can act as primary plateaus. Fig. 10(c) presents a steel fiber serving as support for a secondary plateau while Fig. 10(d) shows several particles of different natures forming spaces among them for debris to fill. Presence of these materials is corroborated by EDX on the SEM image from Fig. 10(c)in Fig. 11.

Areas showing one type of structure or another are probably zones in which a more severe wear regime is observed or wear conditions are mild and such that allow the formation of agglomerates of debris in

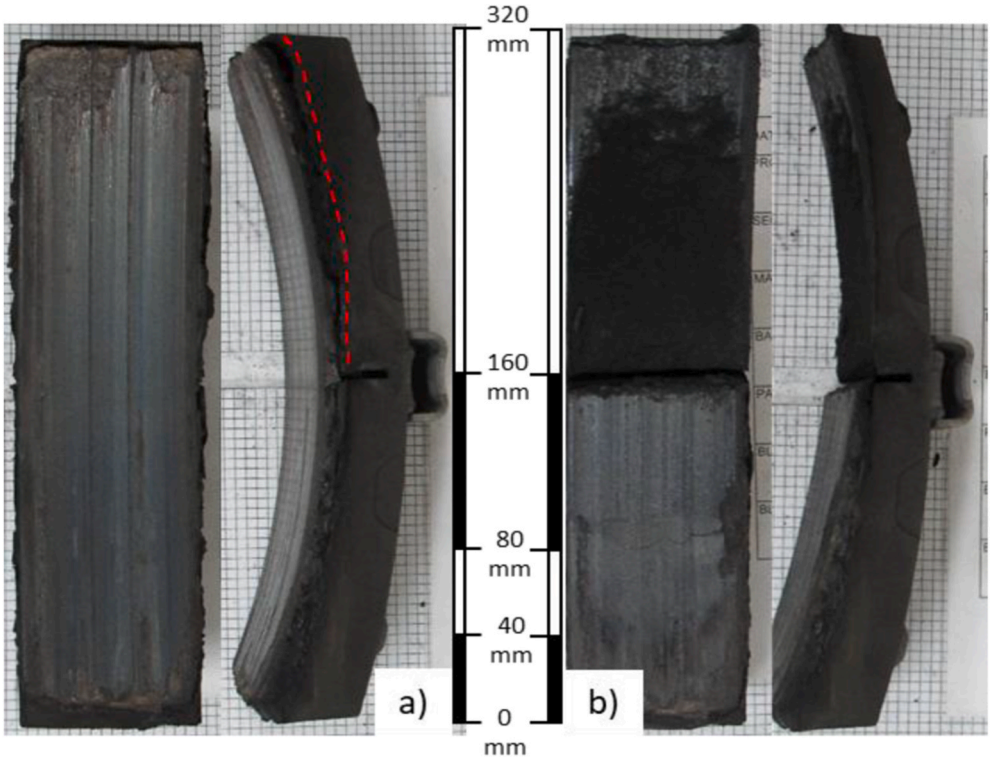

Fig. 9. Pictures of material SW after (a) the drag brake and (b) the thermal phase.

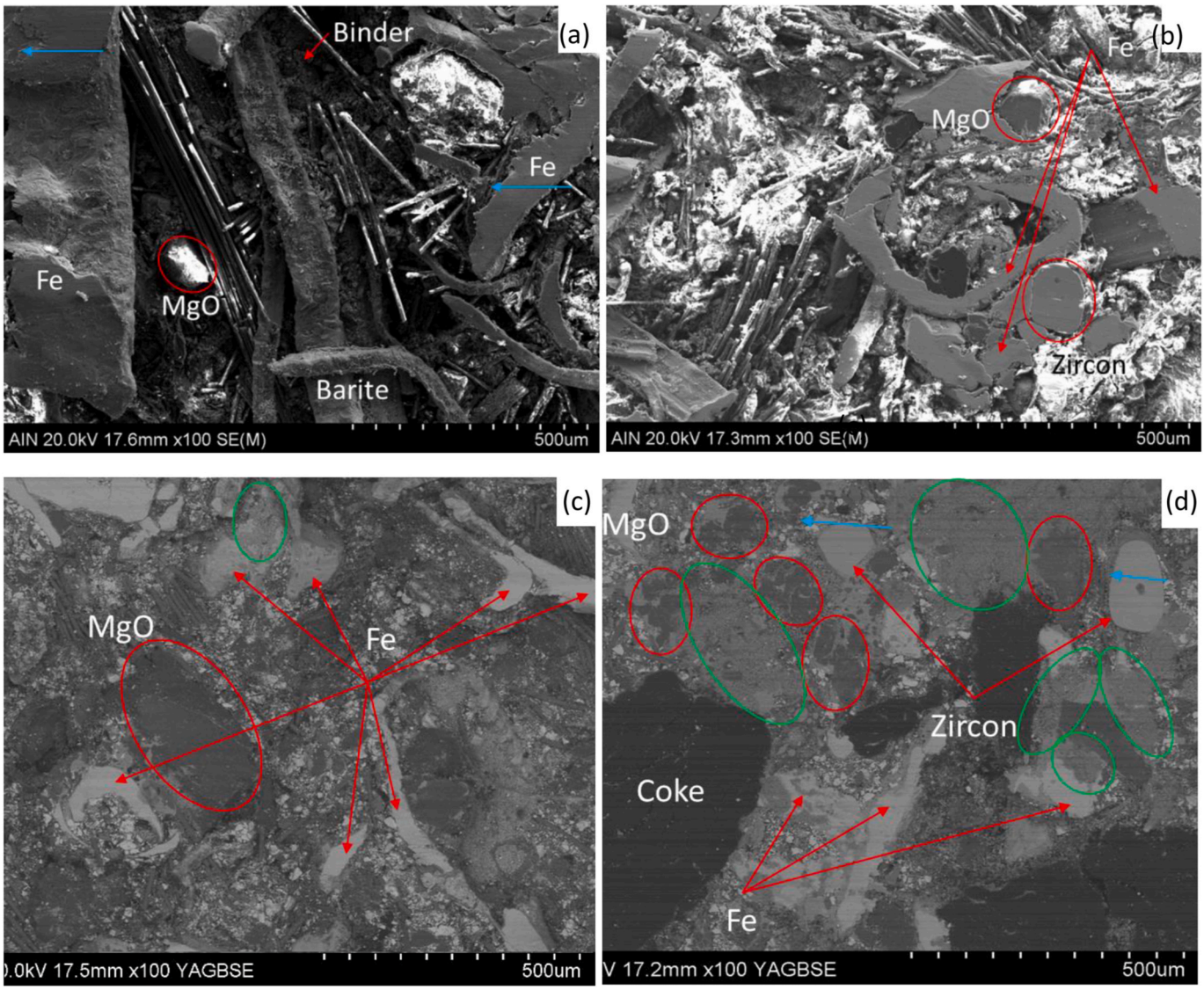

Fig. 10. SEM pictures of worn surfaces of (a) control sample, (b) AF material, (c) PAN material and (d) SW material.

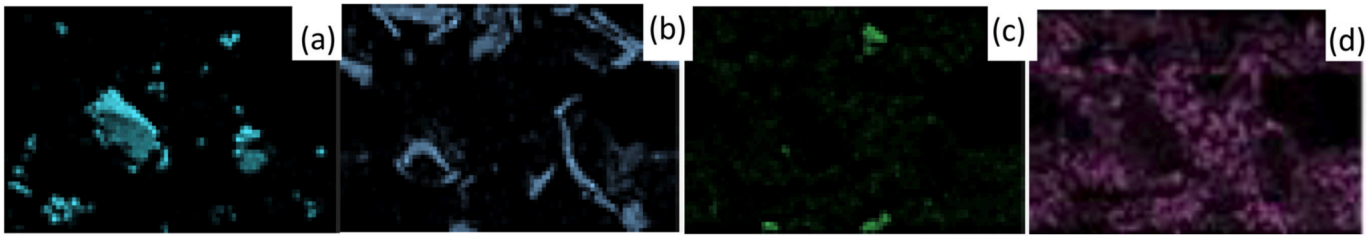

Fig. 11. Element identification by EDX on SEM picture from Fig. 10(c): Magnesium (a), iron (b), zirconium (c) and barium (d).

secondary plateaus. When a wear regime is more severe, the material wearing off the block's surface is larger and there are not enough fixed points and relieves so that debris can pile up and compress against. On the other hand, when particles such as steel fibers provide a support for debris to start compacting around, secondary plateaus are more easily evidenced. The appearance of zones presenting just primary or primary and secondary plateaus on the same friction body has been previously evidenced in full-scale railway dynamometer tests (Monreal et al., 2021a), and it is attributed to an uneven distribution of pressure over the brake shoe friction surface (Barros et al., 2019). In a full-scale friction test, only the overall braking pressure is controlled and deviations such as a slight change in position of the block on the wheel tread can lead to a different adjustment between the two items. This type of happenings does not represent differences at a macroscopic scale, but can represent the distribution of higher loads on determined micro areas which will find their plateau structure more severely affected.

As reported in literature, it often occurs that a tribofilm is generated during braking depending on the conditions of the event. It has also been suggested that one of the mechanisms for this tribofilm formation is the compaction and bonding of wear products upon the first body surfaces

(Österle and Dmitriev, 2016). This particular case, in the form of a well-stablished third body layer was evidenced in a previous work studying the same friction materials in a mid-scale dynamometer at very less demanding conditions (Monreal et al., 2021b). It seemed in that case that Godet's concept of a third body layer covering the first body surfaces applied (Godet, 1984). The presence of this type of third body layer, rich in iron oxide (Barros et al., 2019; Monreal et al., 2021a, 2021b), has been linked to a stabilization of the friction coefficient (Barros et al., 2019). In the case of the present work only relatively isolated agglomerates of wear product forming secondary plateaus were evidence as explained before in relation with Fig. 10. This has been reported to also happen on brake discs (Barros et al., 2019). It is hypothesized that, while the real contact between the two friction bodies occur at the contact plateaus at a microscopic level, something similar could be happening at a larger scale when dealing with large friction surfaces (such as those of Bg brake shoes), where certain zones of the blocks' surface are the ones that actually take part in the braking at a given time. The successive wear and change on these zones could explain the variation of the instantaneous friction coefficient that has been described in the normal brake stops at a full-scale dynamometer (Monreal et al., 2021a). This fact could as well be linked to the heterogeneously distributed tribofilms reported by Barros et al. that can vary depending on the normal load (Barros et al., 2016). On the contrary, when the braking conditions are such that the whole brake surface is really a part of the braking event, these successive changes would not happen and a more stable friction coefficient should be observed. This case was reached right after the drag brake phase (Fig. 9). Although it was not evidenced by SEM, it is known that certain components of the brake can trap wear product and debris by melting during the brake application, helping stabilize a relatively thick third body layer (Cox, 2012a). This seems to have happened with the softened rubber component of the blocks, which even got to flow and fill the blocks' groove, and this could explain the very stable instantaneous friction coefficient that most of the friction materials presented during the final 6 min of the drag brake application. It is proposed to further study this happening by SEM testing the brake shoes after the drag brake to analyze the wear product microstructure.

In general, the microstructure suggesting a wear regime between mild and severe on the blocks tested is coherent with preliminary tests run on the same friction materials on a smaller scale dynamometer (Monreal et al., 2021b). In that case the testing conditions were less demanding as it can be seen by checking the wear rates. A microstructure consisting of secondary plateaus and a well-stablished third body layer was then evidenced, in contrast with what has been reported after the full-scale dynamometer tests.

In addition to these observations, the distribution of other components can be reported. The binder is often seen in the background in the form of dark, granulated matter as shown in Fig. 10(a). Barite can also be seen spread over areas that not yet have been affected by friction. In the same image barite can be seen covering a steel fiber at the bottom. This particular component, barite, being a soft filler, it often removed from the surface of the brake shoe to a certain degree. This phenomenon is evidenced in the EDX results in Fig. 12. When comparing the sum spectrum of a non-tested surface (in Fig. 12(a) for material AF and in Fig. 12(b) for sample SW) with that of a tested area (Fig. 12(c) and (d) for the same materials respectively) peaks of Ba and S among other dramatically decrease. In contraposition, peaks corresponding to Fe (steel fiber), Mg or Zr grow larger. These are the components that have been found to form primary plateaus.

3.5. Life Cycle Assessment results

The LCA results are presented in this subsection. First, the results under ReCiPe methodology will be shown, followed by the ones obtained under CML methodology. Table 9 shows the environmental impact under ReCiPe 2016 Endpoint per unit of brake block.

Focusing on the materials, for all the brake blocks, most of the impact is created by the use of NBR (between 26.7 and 30.8% of the environmental impact in a brake block created by raw materials), followed by steel fibers (between 24.7 and 28.4%), glass fibers (between 9.6 and 11%) and magnesium oxides (between 9.4 and 10.8%). Regarding the organic fibers, aramid generates the higher environmental impact (13% of the environmental impact created by raw materials), followed by PAN (4.6%). On the other hand, cellulose fiber only supposes 4.2% of the environmental impact created by raw materials, where as in the brake block manufactures with sheep wool, Latxa fibers only contribute to 0.01%.

Table 10 shows the environmental impact per unit of brake block under CML-IA baseline v3.05 methodology. With this methodology, on average, materials generate 74% of the overall impact, followed by the manufacturing processes, which create, on average 21%. Transportations only account for approximately 5% of the impact. However, a more detailed analysis on each environmental impact categories allows for further information.

- Abiotic depletion: most of the impact are created by the different manufacturing processes (around 40% of the total impact in this

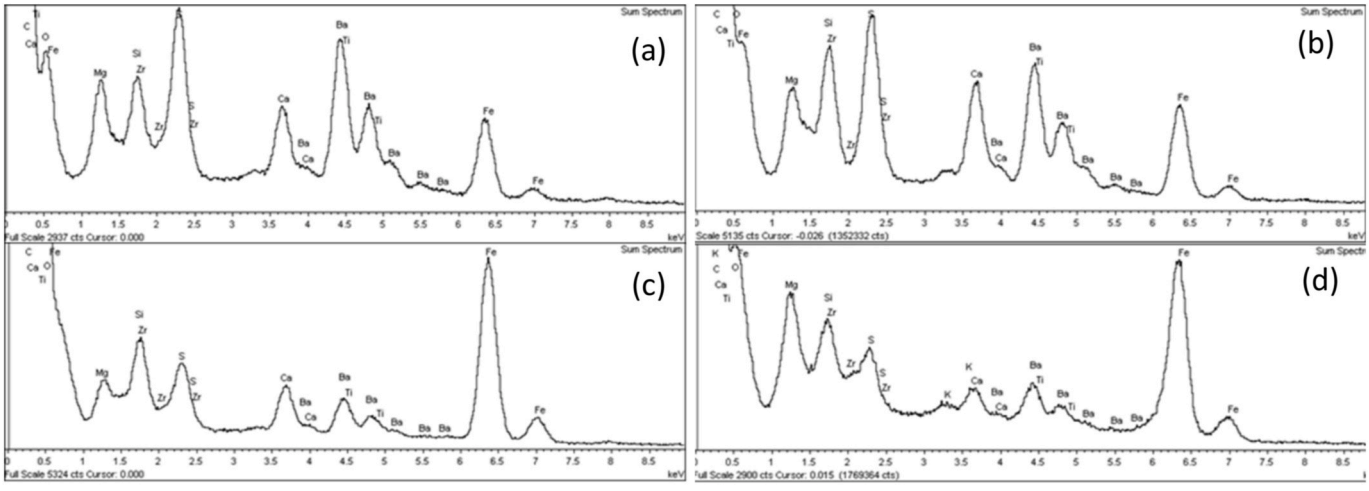

Fig. 12. EDX sum spectra of (a) AF material (non-worn surface), (b) SW material (non-worn surface), (c) AF material (worn surface) and (d) SW material (worn surface).

Table 9
Environmental impact per unit of brake block under ReCiPe 2016 Endpoint (H/A) World 2010 v1.03

Impact category	Unit	Friction material 0	Friction material AF	Friction material CF	Friction material PAN	Friction material SW
ReCiPe EndPoint (H/A)	mPt	350,7	356,8	328,0	336,6	331,2

Under ReCiPe methodology, materials generate between 77.5 and 79.4% of the overall impact, followed by the manufacturing processes, which create between 15.9 and 17.3%. Transportations only account for approximately 5% of the impact.

Table 10
Environmental impact per unit of brake block under CML-IA baseline v3.05 methodology.

Impact category	Unit	Friction material 0	Friction material AF	Friction material CF	Friction material PAN	Friction material SW
Abiotic depletion	kg Sb eq	1,299E-05	1,240E-05	1,248E-05	1,214E-05	1,228E-05
Abiotic depletion (fossil fuels)	MJ	1,061E+02	1,103E+02	9,877E+01	1,058E+02	9,989E+01
Global warming (GWP100a)	kg CO2 eq	8,018E+00	8,469E+00	7,472E+00	7,811E+00	7,555E+00
Ozone layer depletion (ODP)	kg CFC-11 eq	4,751E-07	4,482E-06	4,513E-07	4,694E-07	4,530E-07
Human toxicity	kg 1,4-DB eq	3,816E+00	3,623E+00	3,570E+00	3,547E+00	3,596E+00
Fresh water aquatic ecotox.	kg 1,4-DB eq	3,673E+00	3,415E+00	3,460E+00	3,436E+00	3,488E+00
Marine aquatic ecotoxicity	kg 1,4-DB eq	1,144E+04	1,056E+04	1,071E+04	1,067E+04	1,081E+04
Terrestrial ecotoxicity	kg 1,4-DB eq	2,232E-02	2,123E-02	2,145E-02	2,139E-02	2,153E-02
Photochemical oxidation	kg C2H4 eq	2,669E-03	2,750E-03	2,484E-03	2,560E-03	2,513E-03
Acidification	kg SO2 eq	3,432E-02	3,645E-02	3,235E-02	3,349E-02	3,260E-02
Eutrophication	kg PO4— eq	1,103E-02	1,069E-02	1,035E-02	1,045E-02	1,044E-02

Analyzing CML results for each environmental impact category shows for more relevant information.

category), which are similar for the five brake blocks, and by the use of glass fibers (between 20 and 22% of the impact)

- Abiotic depletion (fossil fuels): The use of NBR is relevant in this category, generating between 37 and 43% of the impact, followed by the manufacturing processes, with averaging 17%. For the AF block, aramid supposes 11.5% of the impact, whereas for the PAN block, PAN fibers create 7.1% of the impact.
- Global warming (GWP100a): For this category, again NBR is the most relevant material (between 25 and 30% of the impact), followed by the manufacturing processes (approximately 21%), steel fibers, which create between 16 and 19% of the impact; and magnesium oxide (around 7%). For the AF block, aramid creates 12.8% of the impact, whereas for the PAN block, PAN fibers create 4.9% of the impact.
- Ozone layer depletion (ODP): For all the materials but the AF, manufacturing generates between 38 and 40%, followed by the transportations, which on average create 17% on the impact. However, for the AF material, the production of aramid fiber creates 90% of the total impact, creating an overall impact in this category almost 10 times higher than the other alternative.
- Human toxicity: Manufacturing processes are responsible for approximately 24% of the impact in this category, followed by phenolic resin, 21%, and steel and glass fibers (15 and 12% respectively)
- Fresh water aquatic ecotoxicity: For this category the manufacturing processes create (on average) 55% of the impact, followed by the use of steel fibers and NBR, with each creating approximately 11% of the impact. Magnesium oxide generate around 8.2%.
- Marine aquatic ecotoxicity: Similarly, to Fresh water aquatic ecotoxicity, the manufacturing processes generate (on average) 57% of the impact, trailed by the use of NBR and steel fibers, with 15 and 9% of the impact, respectively
- Terrestrial ecotoxicity: Almost 72% of the impact in this category are created by the manufacturing processes, mainly electricity consumption. Around 10% of the impact is created by the use of steel fibers, followed by magnesium oxide, with approximately 5%
- Photochemical oxidation: Steel fibers generate between 27 and 32% of the total impact, followed by the manufacturing processes (18.5%), and NBR (between 17.7 and 20.1%)
- Acidification: Manufacturing processes create between 30.3 and 34.2% of the impact, followed by NBR (17.8–20.8%) and steel fibers (12.8–15%)
- Eutrophication: As in previous categories, the manufacturing processes generate on average 38% of the impact, followed by steel fibers (around 20%) and NBR (approximately 10%)

Cellulose and Latxa sheep wool fibers by themselves create very low impacts under all CML environmental impact categories. Cellulose, on average for all the categories supposes 0.55% of the impact, whereas sheep wool creates around 0.01%. Therefore, the main differences between materials are created, not by the natural fibers, but due to the differences in the rest of the composition. The use of natural fibers helps to reduce the amounts of NBR, steel and glass fibers and magnesium oxide, which are the materials that generate most of the environmental impact, therefore the lower amounts used reduce the overall impact created by the brake blocks.

4. Conclusions

Railway brake shoes using latxa sheep wool fibers were produced and tested in comparison to others including three different, well-known organic fibers: aramid, cellulose and polyacrylonitrile (PAN) fibers. It was concluded that the natural, environmentally-friendly sheep wool fiber led to similar friction levels and dependence with temperature than the other fibers, It also presented good recovery values and no significant differences were evidenced in the wear mechanism by SEM analysis.

- Sheep wool is a suitable organic fiber to be used in the manufacture of railway brake shoes, as it leads to similar friction coefficients to those of materials including other fibers. It also led to wear rates between the ones of the cellulose fiber and PAN fiber.
- The inclusion of any kind of organic fiber seemed to help achieve a stable friction coefficient during the bedding phase.
- No large variations on friction performance were observed due to the nature of the organic fibers. Material 0 showed a more stable friction, especially in wet conditions. Material AF presented the most varying friction coefficient with speed and force.
- After the continuous brake application (drag brake) the different organic fibers gave significant differences in recovery. Material SW showed the closest recovery to 100%. The thermal phase did not bring significant differences in relation to recovery of the fibers, although all of them sowed values closer to 100 than material 0.

- The wear mechanism and the failure sequence was independent on the nature of the organic fiber added. Instead, the fibers marked the magnitude of the wear during the most demanding phases of the test.
- Friction material using cellulose presented the highest wear rate. The sheep wool generally led to a wear rate close to that of PAN fiber.
- SEM analysis found no evidences of organic fibers modifying the wear mechanism, which was characterized for all tested samples as comprising of only primary and both primary and secondary plateaus in different areas analyzed. These structures are attributed to a non-perfect braking pressure distribution at a microscopic level.
- From an environmental perspective, the manufacturing of brake blocks using sheep wool fibers offers comparable, although slightly higher impacts than cellulose. Overall, cellulose, PAN and sheep wool show slightly lower environmental impacts that the base material or than aramid fiber.
- The main differences between both materials with natural fibers are created, not by the natural fibers, but due to the differences in the rest of the composition. The use of natural fibers helps to reduces the amounts of NBR, steel and glass fibers, which are the materials that generate most of the environmental impact, therefore reducing the overall impact created by the brake blocks. Therefore, Latxa sheep wool offers a good balance between low cost, adequate wear rates and environmental impact, making it a compelling substitute for cellulose fibers.

Author contributions

Pablo Monreal: Term, Conceptualization, Methodology, Investigation, Data curation, Resources, Writing Original Draft. Daniel Elduque: Methodology, Investigation, Data curation, Writing Original Draft. David López: Supervision, Project administration. Iranzu Sola: Investigation. Javier Yaben: Investigation. Isabel Clavería: Term, Writing Reviewing & Editing.

Declaration of competing interest

The authors declare that they have no known competing financial interests or personal relationships that could have appeared to influence the work reported in this paper.

Data availability

Data will be made available on request.

Acknowledgements

Authors gratefully acknowledge the help and support provided by the Quality Assurance Laboratory and the R&D Department at Knorr-Bremse Pamplona. Specially the prototyping and friction testing areas whose collaboration made possible the present research work.

References

Aranganathan, N., Mahale, V., Bijwe, J., 2016. Effects of aramid fiber concentration on the friction and wear characteristics of non-asbestos organic friction composites using standardized braking tests. Wear 354, 69–77. https://doi.org/10.1016/j.wear.2016.03.002.

Barros, L.Y., Neis, P.D., Ferreira, N.F., Pavlak, R.P., Masotti, D., Matozo, L.T., Sukumaran, J., De Baets, P., Andó, M., 2016. Morphological analysis of pad–disc system during braking operations. Wear 353, 112–121. https://doi.org/10.1016/j.wear.2016.02.005.

Barros, L.Y., Poletto, J.C., Buneder, D., Neis, P.D., Ferreira, N.F., Pavlak, R.P., Matozo, L.T., 2019. Effect of pressure in the transition between moderate and severe wear regimes in brake friction materials. Wear 438–439. https://doi.org/10.1016/j.wear.2019.203112.

Batchelor, C., Carey, E., 1954. Friction Facts, Fortes, and Foibles. Society of Automotive Engineers, Warrendale, PA. Technical Paper No. 540030.

Batista, F., Almeida, F., Vieira da Silva, M.A., 2022. Environmental performance analysis of railway infrastructure using life cycle assessment: selecting pavement projects based on global warming potential impacts. J. Clean. Prod. 365, 132558 https://doi.org/10.1016/j.jclepro.2022.132558.

Bijwe, A.N.J., 2016. Development of copper-free eco-friendly brake-friction material using novel ingredients. Wear 352-353, 79–91.

Bowden, ScD., F. P., 1951. The influence of surface films on the friction, adhesion, and surface damage of solids. Ann. N. Y. Acad. Sci. 53 (4), 805–823. https://doi.org/10.1111/j.1749-6632.1951.tb54239.x.

Cai, P., Li, Z., Wang, T., Wang, Q., Effect of Aspect Ratios of Aramid Fiber on Mechanical and Tribological Behaviors of Friction Materials. Tribol. Int. 92, 109–116. https://doi.org/10.1016/j.triboint.2015.05.024..

Chen, H., Ishida, M., Namura, A., Baek, K.S., Nakahara, T., Leban, B., Pau, M., 2011. Estimation of wheel/rail adhesion coefficient under wet condition with measured boundary friction coefficient and real contact area. Proc. 8th Int. Conf. Contact Mech. Wear Rail Wheel Syst. Florence 271 (1), 32–39. https://doi.org/10.1016/j.wear.2010.10.022.

Consultants, Pre, 2020. SimaPro 9 Database Manual, vol. 2020. Methods Library.

Cox, R., 2012a. Chapter 5 friction material manufacturing methods. In: Engineered Tribological Composites. SAE, pp. 85–112.

Cox, R., 2012b. Chapter 13 organic fiber: in engineered tribological composites. SAE 247–266.

Del Pero, F., Delogu, M., Pierini, M., Bonaffini, D., 2015. Life Cycle Assessment of a heavy metro train. J. Clean. Prod. 87, 787–799. https://doi.org/10.1016/j.jclepro.2014.10.023.

Dong, Y.H., Ng, S.T., 2014. Comparing the midpoint and endpoint approaches based on ReCiPe – a study of commercial buildings in Hong Kong. Int. J. Life Cycle Assess. 19 (7), 1409–1423. https://doi.org/10.1007/s11367-014-0743-0.

El-Tayeb, N.S.M., Liew, K.W., 2007. Effect of water spray on friction and wear behaviour of noncommercial and commercial brake pad materials. J. Mater. Process. Technol. 208 (1), 135–144. https://doi.org/10.1016/j.jmatprotec.2007.12.111.

EL-Tayeb, N.S.M., Liew, K.W., 2009. On the dry and wet sliding performance of potentially new frictional brake pad materials for automotive industry. Wear 266 (1), 275–287. https://doi.org/10.1016/j.wear.2008.07.003.

Eriksson, M., Jacobson, S., 2000. Tribological surfaces of organic brake pads. Tribol. Int. 33 (12), 817–827. https://doi.org/10.1016/S0301-679X(00)00127-4.

Eriksson, M., Bergman, F., Jacobson, S., 2002. On the nature of tribological contact in automotive brakes. Wear 252 (1), 26–36. https://doi.org/10.1016/S0043-1648(01)00849-3.

Fei, J., Luo, W., Li, H., Huang, J., Ouyang, H., Wang, H., 2015. Effects of NBR particle size on performance of carbon fiber–reinforced paper-based friction. Mater. Tribol. Trans. 58 (6), 1012–1020. https://doi.org/10.1080/10402004.2015.1034906.

Gibson, D.W., Taccini, C.J., 1989. Carbon/carbon friction materials for dry and wet brake and clutch applications. SAE Int. https://doi.org/10.4271/890950. Technical paper 890950.

Godet, M., 1984. The third-body approach: a mechanical view of wear. Wear 100 (1), 437–452. https://doi.org/10.1016/0043-1648(84)90025-5.

Gradin, K.T., Åström, A.H., 2020. Comparative life cycle assessment of car disc brake systems—case study results and method discussion about comparative LCAs. Int. J. Life Cycle Assess. 25, 350–362. https://doi.org/10.1007/s11367-019-01704-9.

Hong, U.S., Jung, S.L., Cho, K.H., Cho, M.H., Kim, S.J., Jang, H., 2009. Wear mechanism of multiphase friction materials with different phenolic resin matrices. Wear 266 (7), 739–744. https://doi.org/10.1016/j.wear.2008.08.008.

Huang, X., 2009. Fabrication and properties of carbon fibers. Mater 2 (4), 2369–2403. https://doi.org/10.3390/ma2042369.

Huijbregts, M.A.J., Steinmann, Z.J.N., Elshout, P.M.F., Stam, G., Verones, F., Vieira, M.D.M., et al., 2016. ReCiPe 2016 – A Harmonized Life Cycle Impact Assessment Method at Midpoint and Endpoint Level. Report I: Characterization. Natl Inst Public Heal Environ, p. 194.

ISO, 2006a. ISO International Organization for Standardization ISO 14040:2006 Environmental Management — Life Cycle Assessment — Principles and Framework.

ISO, 2006b. Environmental Management — Life Cycle Assessment — Requirements and Guidelines. ISO International Organization for Standardization ISO 14044:2006.

Jara, D.C., Jang, H., 2019. Synergistic effects of the ingredients of brake friction materials on friction and wear: a case study on phenolic resin and potassium titanate. Wear 430–431, 222–232. https://doi.org/10.1016/j.wear.2019.05.011.

Jordan, B., 2020. May 19). 50 toneladas de lana de oveja latxa del Valle de Baztán se convierten en abono orgánico. Cadena SER https://cadenaser.com/emisora/2020/05/19/radio_pamplona/1589894818_624932.html.

Kalel, L., Bhatt, B., Darpe, A., Bijwe, J., 2021. Copper-free Brake-Pads: A Break-Through by Selection of the Right Kind of Stainless Steel Particles. Wear. 464-465. https://doi.org/10.1016/j.wear.2020.203537.

Kato, T., Magario, A., 1994. The wear of aramid fiber reinforced brake pads: the role of aramid fibers. Tribol. Trans. 37 (3), 559–565. https://doi.org/10.1080/10402009408983329.

Kim, S.J., Cho, M., Lim, D., Jang, H., 2001. Synergistic effects of aramid pulp and potassium titanate whiskers in the automotive friction. Mater. Wear. 251, 1484–1491. https://doi.org/10.1016/S0043-1648(01)00802-X.

Krause, J., 2015. The potential of an environmentally friendly business strategy — research from the Czech republic. Int. J. Eng. Bus. Manag. 7, 6. https://doi.org/10.5772/60064.

Kumar, M., Bijwe, J., 2010. Role of different metallic fillers in non-asbestos organic (NAO) friction composites for controlling sensitivity of coefficient of friction to load and speed. Spec. Issue Second Int. Conf. Adv. Tribol. ICAT2008 43 (5), 965–974 https://doi.org/10.1016/j.triboint.2009.12.062.

Kumar, M., Kumar, A., 2020. Thermomechanical analysis of hybrid friction composite material and its correlation with friction braking performance. Int. J. Polym. Anal. Char. 25 (2), 65–81. https://doi.org/10.1080/1023666X.2020.1746543.

Kunz, A., Meyer, M., Göcze, C., Martinotto, L., Lieberherr, W., 2019. Strategy Panel. Eurobrake 2019. Dresden, Germany.
Laguna-Camacho, J.R., Juárez-Morales, G., Calderón-Ramón, C., Velázquez-Martínez, V., Hernández-Romero, I., Méndez-Méndez, J.V., Vite-Torres, M., 2015. A study of the wear mechanisms of disk and shoe brake pads. Eng. Fail. Anal. 56, 348–359. https://doi.org/10.1016/j.engfailanal.2015.01.004.
Li, Z., Liu, B., Haijuan, K., Yu, M., Qin, M., Teng, C., 2018. Layer-by-Layer self-assembly strategy for surface modification of aramid fibers to enhance interfacial adhesion to epoxy resin. Polymers 10, 820. https://doi.org/10.3390/polym10080820.
Lin, J., Lobo, A., Leckie, C., 2017. Green brand benefits and their influence on brand loyalty. Market. Intell. Plann. 35, 425–440. https://doi.org/10.1108/MIP-09-2016-0174.
Madeswaran, A., Natarajasundaram, B., Ramamoorthy, B., 2016. Reformation of eco-friendly automotive brake pad by using natural fibre composites. SAE Int. https://doi.org/10.4271/2016-28-0164. Technical Paper 2016-28-0164.
Manoharan, S., Vijay, R., Suresha, B., 2019. Tribological characterization of recycled basalt-aramid fiber reinforced hybrid friction corn posites using grey-based Taguchi approach. Mater. Res. Express 6 (6), 065301. https://doi.org/10.1088/2053-1591/ab07ce.
Matějka, V., , Simha Martynková, G., Yuning, M., Yafei, L., 2009. Semimetallic brake friction materials containing ZrSiO4: friction performance and friction layers evaluation. J. Compos. Mater. 43 (13), 1421–1434. https://doi.org/10.1177/0021998308104730.
Matsumori, T., Goto, Y., , Sugiura, N., Abe, K., Osawa, Y., Akita, Y., Wakamatsu, S., Okayama, K., Kosaka, K., 2016. Friction coefficient variation mechanism under wet condition in disk brake (variation mechanism contributing wet wear debris). SAE Int. J. Passeng. Cars - Mech. Syst. 9 (3), 1227–1234. https://doi.org/10.4271/2016-01-1943.
Menapace, C., Leonardi, M., Matějka, V., Gialanella, S., Straffelini, G., 2018. Dry sliding behavior and friction layer formation in copper-free barite containing friction materials. Wear 398, 191–200. https://doi.org/10.1016/j.wear.2017.12.008.
Monreal, P., Clavería, I., Arteta, P., Rouzaut, T., 2021a. Effect of modified novolac resins on the physical properties and friction performance of railway brake blocks. Tribol. Int. 154, 106722 https://doi.org/10.1016/j.triboint.2020.106722.
Monreal, P., Oroz, J., Gutiérrez, K., Clavería Ambroj, I., 2021b. Natural latxa sheep wool as an environmentally friendly substitute for specific organic fibers in railway friction materials: a preliminary approach. Tribol. Trans. 64 (10), 1–13. https://doi.org/10.1080/10402004.2021.1939210.
Nukumizu, K., Kobayashi, T., Abe, T., Unno, M., 2008. Study of the formulation mechanism for metal pick-up on the frictional surface of a disc brake pad. SAE Int. https://doi.org/10.4271/2008-01-2541. Technical Paper 2008-01–2541.
Orecchini, F., Valitutti, V., Vitali, G., 2012. Industry and academia for a transition towards sustainability: advancing sustainability science through university–business collaborations. Sustain. Sci. 7 (S1), 57–73. https://doi.org/10.1007/s11625-011-0151-3.
Ospina, D., Villegas, V.E., Rodriguez-Leguizamon, G., Rondon-Lagos, M., 2019. Analyzing biological and molecular characteristics and genomic damage induced by exposure to asbestos. Cancer Manag. Res. 11, 4997–5012. https://doi.org/10.2147/CMAR.S205723.
Österle, W., Dmitriev, A., 2016. The role of solid lubricants for brake friction materials. Lubricants 4 (1), 5. https://doi.org/10.3390/lubricants4010005.
Park, J., Song, W., Gweon, J., Seo, H., Lee, J.J., Jang, H., 2021. Size effect of zircon particles in brake pads on the composition and size distribution of emitted particulate matter. Tribol. Int. 160, 106995.
Prasenjit, M., Sanjeev, M., Praveen, S., 2021. Epigenetics in lead toxicity: new avenues for future research. Indian J. Clin. Biochem. 36, 129–130. https://doi.org/10.1007/s12291-021-00969-y.
Saffar, A., Shojaei, A., 2012. Effect of rubber component on the performance of brake friction materials. Wear 274–275, 286–297. https://doi.org/10.1016/j.wear.2011.09.012.
Sai Krishnan, G., Jayakumari, L.S., Ganesh Babu, L., Suresh, G., 2019. Investigation on the physical, mechanical and tribological properties of areca sheath fibers for brake pad applications. Mater. Res. Express 6 (8), 085109. https://doi.org/10.1088/2053-1591/ab2615.
Sanitate, F., Schmitt, O., 2008. An investigation of metal pick-up generation on passenger car brake pads in correlation with deep rotor scoring. SAE Int. https://doi.org/10.4271/2008-01-2540. Technical Paper 2008-01–2540.
Satapathy, B.K., Bijwe, J., 2004. Performance of friction materials based on variation in nature of organic fibres Part I. Fade and recovery behaviour. Wear 257 (5–6), 573–584. https://doi.org/10.1016/j.wear.2004.03.003.
Satapathy, B.K., Bijwe, J., 2006. Composite friction materials based on organic fibres: sensitivity of friction and wear to operating variables. Compos. Part Appl. Sci. Manuf. 37 (10), 1557–1567. https://doi.org/10.1016/j.compositesa.2005.11.002.
Shalwan, A., Yousif, B.F., 2013. In State of Art: mechanical and tribological behaviour of polymeric composites based on natural fibres. Mater. Des. 48, 14–24. https://doi.org/10.1016/j.matdes.2012.07.014.
Shimer, G., 1883. Brake shoe. United States Patent No. 272911, filed November 28, 1882, and issued February 27, 1883.
Shin, M.W., Kim, Y.H., Jang, H., 2014. Effect of the abrasive size on the friction effectiveness and instability of brake friction materials: a case study with zircon. Tribol. Lett. 55 (3), 371–379. https://doi.org/10.1007/s11249-014-0361-9.
Singh, T., Rathi, M.K., Fekete, G., 2019. Application of waste tire rubber particles in non-asbestos organic brake friction composite materials. Mater. Res. Express 6 (3), 035703. https://doi.org/10.1088/2053-1591/aaf684.
Singh, T., Patnaik, A., Chauan, R., Biro, I., Janosi, E., Fekete, G., 2020. Performance assessment of phenolic-based non-asbestos organic brake friction composite materials with different abrasives. Acta Polytech. Hungarica. 17 (5), 49–67.
Spokes, 1947. Friction element. United states patent No. 2428298, filed November 16, 1942, and issued September 30.
Sugözü, B., Dağhan, B., 2016. Effect of BaSO4 on tribological properties of brake friction materials. Int. J. Innov. Res. Sci. Eng. Technol. 5 (12), 30–35.
Surojo, E., Ariawan, D., Arsada, R., Muhayat, N., Raharjo, W.W., Smaradhana, D.F., 2019. Effect of nitrile butadiene rubber (NBR) on mechanical and tribological properties of composite friction brakes. Tribol. Ind. 41 (4), 516–525. https://doi.org/10.24874/ti.2019.41.04.05.
Talib, R.J., Amri, M.H., Selamat, M.A., Basri, M.H., Ismail, N.I., Sulaiman, Z.S., Jumahat, A., 2017. Adaptability of activated carbon from palm oil kernel shell in the development of brake friction materials. Advanced materials for sustainability and growth. AIP Conf. Proc. 1901, 030020 https://doi.org/10.1063/1.5010485.
Tejada, M., 2020. February 7). Cazadoras térmicas con lana de oveja latxa. El diario vasco. https://www.diariovasco.com/gipuzkoa/cazadoras-termicas-lana-20200207122724-nt.html.
Uibu, T., Oksa, P., Auvinen, A., Honkanen, E., Metsärinne, K., Saha, H., Uitti, J., Roto, P., 2004. Asbestos exposure as a risk factor for retroperitoneal fibrosis. Lancet 363 (9419), 1422–1426. https://doi.org/10.1016/S0140-6736(04)16100-X.
Wernet, G., Bauer, C., Steubing, B., Reinhard, J., Moreno-Ruiz, E., Weidema, B., 2016. The ecoinvent database version 3 (part I): overview and methodology. Int. J. Life Cycle Assess. 21 (9), 1218–1230. https://doi.org/10.1007/s11367-016-1087-8.
Wild, R., 1931. Friction material. United states patent No. 1803448, filed November 29, 1929, and issued May 5, 1931.
Wu, H., Wang, Y., Pindar, D., Ferdani, P., 2011. Interaction between ceramic matrix composite and organic pad materials and its impact on the friction performance. SAE Int. https://doi.org/10.4271/2011-01-2350. Technical paper 2011-01–2350.